Inner hair cell synapse density influences auditory processing

Lingchao Ji[1]; Beatriz C. Borges[1]; David T. Martel[1]; Calvin Wu[1]; M. Charles Liberman[2]; Susan E. Shore[1,3,4,*], Gabriel Corfas[1,*]

[1]Kresge Hearing Research Institute and Dept. of Otolaryngology, Head and Neck Surgery, University of Michigan

[2]Mass.Eye and Ear Infirmary and Harvard Medical School

[3]Biomedical Engineering, University of Michigan

[4]Molecular and Integrative Physiology, University of Michigan

[*] co-senior authors

Corresponding author:

Gabriel Corfas, Ph.D.
Kresge Hearing Research Institute
The University of Michigan
Medical Sciences I Building, Rm. 5428
1150 West Medical Center Drive
Ann Arbor, MI 48109-5616
Tel: 734-615-2222
Email: corfas@med.umich.edu

Acknowledgements: This work was supported in part by NIH/NIDCD R01 DC018500 (GC), NIH/NIDCD R01 DC000188 (MCL), and a grant from the American Tinnitus Association (GC).

Conflict of interest: GC and MCL are scientific founders of Decibel Therapeutics, have equity interest in the company and have received compensation for consulting. SES and DM are scientific founders of Auricle, Inc and have equity interest in the company. Neither company was involved in this study.

Abstract

It has been proposed that inner hair cell (IHC) synaptopathy, i.e., loss of synapses between spiral ganglion neurons and IHCs, leads to hidden hearing loss (HHL), i.e. poor performance on challenging hearing tasks despite a normal audiogram. However, this has only been tested in animals after exposure to noise or ototoxic drugs, which can cause deficits beyond synaptopathy. Furthermore, the impact of supernumerary synapses on auditory processing has not been evaluated. Here, we studied mice in which IHC synapse counts have been increased or decreased by altering neurotrophin 3 (Ntf3) expression in IHC supporting cells. As we previously showed, postnatal Ntf3 knockdown or overexpression reduces or enhances suprathreshold ABR amplitude and IHC synapse density, respectively, without changing cochlear thresholds. Here, we show that IHC synapse density does not influence the acoustic startle reflex or prepulse inhibition, measures of reflexive responses to sound and sensory-motor gating. In contrast, gap-prepulse inhibition, a behavioral test for auditory temporal processing, was increased or reduced according to Ntf3 expression levels. These results indicate that cochlear synaptopathy causes temporal processing deficits, which may be a key contributor to the hearing impairments that define HHL. Furthermore, the improvement in temporal acuity achieved by increasing Ntf3 expression and synapse density suggests a therapeutic strategy for improving hearing in noise for individuals with synaptopathy of various etiologies.

Introduction

The inner hair cells (IHCs) of the mammalian organ of Corti transduce sounds into neural activity through glutamatergic excitatory synapses onto primary auditory neurons, the type I spiral ganglion neurons. These synapses are vulnerable to both aging and noise exposure (1), i.e. even moderate noise exposure and/or normal aging result in loss of IHC synapses (2, 3). This type of deafferentation, a.k.a. cochlear synaptopathy, has been well documented in various mammalian species, including mice (1), guinea pigs (4), rats (5), gerbils (6), chinchillas (7) and in post-mortem human temporal bones (8, 9). Animal-model studies have shown that moderate cochlear synaptopathy caused by noise overexposure or aging causes “hidden hearing loss,” i.e. an auditory neuropathy that manifests as a reduction in suprathreshold amplitudes of the first peak (P I) of the auditory-brainstem response (ABR) without a shift in cochlear thresholds (1).

It has been hypothesized that cochlear synaptopathy leads to neural coding deficits that impair speech discrimination and intelligibility, especially in noisy environments, and to compensatory increases in the “gain” of central circuits that cause hyperacusis and tinnitus (10). Indeed, experiments on animals with noise- or drug-induced cochlear synaptopathy show evidence for persistent gain in central circuits, either in the enhancement of acoustic startle responses (11) or of sound-evoked response rates in neurons from the inferior colliculus or cortex in awake animals (12, 13). Cortical responses from synaptopathic animals also show threshold elevations for detectability of tones in noise without changes in tone detection in quiet (13). However, other studies have failed to find such correlation (14). In human, several studies have shown a relationship between noise-exposure history and reductions in ABR suprathreshold amplitudes among those with normal audiometric thresholds (15), or a correlation between ABR P1 amplitudes and performance on speech-in-noise tasks (16, 17), but direct demonstration of cochlear synaptic loss was lacking. Furthermore, others studies have found no evidence for a direct relationship between hidden hearing loss and impaired speech perception (18).

To explore the impact of cochlear synapse density on auditory function, and to probe the effects of cochlear synaptopathy in the absence of cochlear insults from acoustic overexposure, ototoxic drugs or aging, whose effects may be more widespread than the loss of cochlear synapses, we used transgenic mice in which IHC synapse density can be controlled via altering neurotrophin 3 (Ntf3) expression by IHC-supporting cells (19). We previously showed that altering the levels of supporting-cell Ntf3 expression starting in the neonatal period permanently changes IHC-synapse density, i.e., Ntf3 over-expression increases IHC-synapse numbers and enhances ABR P1 amplitudes, whereas Ntf3 knock-down decreases them (19). Here, we tested the behavioral phenotypes of these transgenic mice, focusing on the acoustic startle reflex and its modulation by prepulse inhibition (PPI) and gap-prepulse inhibition of the acoustic startle (GPIAS). These behaviors have been used to assess stimulus salience, sensory gating and temporal processing (20-25).

We found that gap-inhibition was stronger than normal in animals with increased IHC synapse density (and Ntf3 overexpression) and was worse than normal in animals with decreased synapse density (and Ntf3 knockdown), without any changes in the strength of the acoustic startle itself or its PPI. As seen with noise- or drug-induced loss of synapses, the later ABR peaks, originating from auditory brainstem and midbrain nuclei, were unchanged after NTf3 knockdown, despite a decrease in P1 amplitudes, suggesting a compensatory increase in central gain. In NTf3 overexpressors, all ABR waves were enhanced, suggesting there are no mechanisms for central gain reduction after a peripheral gain of function. Together, these results are consistent with the notion that enhancing IHC-synapse density could lead to a general enhancement of temporal processing abilities.

Results

Regulating IHC synapse density and sound-evoked auditory nerve activity via Ntf3 knock-down or over-expression.

To modify the levels of Ntf3 expression by IHC supporting cells, we used cell-specific inducible gene recombination as in prior studies (19). Briefly, the Plp1-CreERT transgenic line (26) was used to drive gene recombination in IHC supporting cells via tamoxifen treatment during the neonatal period (27). This CreERT transgene was combined with either conditional Ntf3 KO alleles ($Ntf3^{flox/flox}$) to reduce Ntf3 expression, or an inducible Ntf3 over-expression transgene ($Ntf3^{STOP}$) (19). As controls, we used mice with the conditional Ntf3 alleles without the CreERT transgene.

Between the ages of 8 and 15 weeks, mutant and control mice underwent a variety of behavioral and physiological tests (Fig. 1). At 16 weeks, cochlear tissues were harvested to measure Ntf3 expression levels and the number of synapses per IHC (synapse density).

Quantitative RT-PCR confirmed that cochlear Ntf3 levels were reduced in the $Ntf3^{flox/flox}$:Plp1-$CreER^T$ mice and increased in the $Ntf3^{STOP}$:Plp1-$CreER^T$ mice (Fig. 2A, B). Similarly, expression of VGF mRNA (28), a gene downstream of neurotrophin receptor signaling, was decreased in the cochleas of $Ntf3^{flox/flox}$:Plp1-$CreER^T$ mice (Fig. 2A) and increased in $Ntf3^{STOP}$:Plp1-$CreER^T$ mice (Fig. 2B). Furthermore, there was a correlation between the mRNA levels of Ntf3 and VGF (Fig. 2E), indicating that the changes in Ntf3 expression impact TrkC signaling in the inner ear. Since the Plp1 gene is also expressed in oligodendrocytes in the brain, we measured the levels of Ntf3 and VGF in the cerebral cortex and found a small decrease in Ntf3 mRNA levels in $Ntf3^{flox/flox}$:Plp1-$CreER^T$ mice (Fig. 2C), no change in Ntf3 mRNA in $Ntf3^{STOP}$:Plp1-$CreER^T$, and most importantly, no changes in VGF mRNA levels in the either Ntf3 KO or Ntf3 OE mice (Fig. 2D), indicating that the manipulation of Ntf3 expression in Plp1-expressing cells is unlikely to have a direct effect on the central nervous system.

We analyzed immunostained cochleas to assess the numbers of synapses between IHCs and auditory nerve fibers. Although each auditory nerve fiber contacts a single IHC, each IHC is contacted by numerous auditory nerve fibers. Each of these glutamatergic synaptic contacts can be identified as a closely apposed pair of puncta in cochleas immunostained for CtBP2, a major component of the presynaptic ribbon, and GluA2, the glutamate receptor subunit most strongly expressed in the post-synaptic plaque on the auditory nerve terminal (Fig. 3). In a normal mouse, the mean number of synapses per IHC follows an inverted U-shaped function, peaking in mid-cochlear regions at a value of roughly 20 synapses per IHC. Here, after normalizing the synaptic counts to the mean peak value in controls, we observed that reduced Ntf3 levels decreased IHC synapse density in the basal half of the cochlea by as much as 20%, as previously reported (19), while increased Ntf3 levels increased IHC synapse density in the same cochlear regions by as much as 30% (Fig. 3A, B).

At 8 weeks of age, we assessed cochlear function by measuring distortion product otoacoustic emissions (DPOAEs), which reflect outer hair cell function, and ABRs, which reflect the summed responses of the auditory nerve and several higher auditory centers (29). While P1 reflects synchronous activity of auditory-nerve fibers, the second peak (P II) is dominated by contributions from cochlear-nucleus bushy cells, and later waves represent bushy-cell targets in the superior olivary complex and inferior colliculus (29-33).

These recordings confirmed, as reported earlier (19), that reduced Ntf3 expression by IHC supporting cells reduces ABR P1 amplitudes cells without changing ABR and DPOAE thresholds, while increasing Ntf3 leads to normal thresholds with increased P1 amplitudes (Fig. 2). Whereas P1 amplitude was reduced in the Ntf3 KOs, later ABR peak amplitudes were normal (Fig 3A), suggesting that decreased sound-evoked activity of the auditory nerve leads to increased gain in higher auditory centers, as seen after noise- or drug-induced synaptic loss (5,

11). In contrast, Ntf3 overexpression resulted in increased amplitudes for all ABR peaks (Fig. 3B), suggesting that increased IHC synapse density amplifies sound-evoked signaling along the ascending auditory pathway. All peak latencies were normal in both mutants (Fig. 4 A, B), suggesting that conduction velocity was not affected.

IHC synapse density does not influence acoustic startle reflex or prepulse inhibition.

To examine the impact of IHC synapse density on auditory temporal processing, we first measured the acoustic startle response (34). Baseline movements and the magnitude of the acoustic startle response to the startle pulse were the same for mutant and control mice (Fig. 5A, B), indicating that changes in Ntf3 expression, synapse density and sound-evoked potentials do not affect motor function or the baseline magnitude of the acoustic startle reflex.

We then measured PPI of the acoustic startle. In the PPI paradigm, a low-level acoustic stimulus (prepulse) is presented 50 ms prior to the startle stimulus. In normal mice, the prepulse reduces the startle, quantified as the fractional reduction, i.e., 1 minus the ratio of startle magnitude with and without prepulse. There was no difference between control and mutant mice in PPI (Fig. 5C, D), suggesting that changes in synapse density and associated changes in auditory nerve activity do not affect sensorimotor gating or acoustic salience (23).

IHC synapse density influences gap-prepulse inhibition.

Next, we measured GPIAS, in which a brief silent gap in a continuous background noise is used to inhibit the startle response. GPIAS has been used to examine auditory temporal processing (20, 22, 25, 35), and correlates with speech recognition in humans (36, 37). GPIAS is also quantified as the fractional reduction of startle, i.e., 1 minus the ratio of the startle magnitude with and without a gap.

We presented gaps of different lengths (0, 3, 5, 15, 25, or 50 ms) in a continuous broadband noise (Fig. 6A). Consistent with previous reports (22), shorter gaps elicited less inhibition than longer gaps (Fig. 6B, C). Ntf3-KO mice showed a significant decrease in gap inhibition whereas Ntf3-OE mice showed a significant increase (Fig. 6B, C). Moreover, we found an increase in the gap-detection thresholds of Ntf3-KO mice and a decrease in gap-detection thresholds in Ntf3-OE mice (Fig. 6B, C), indicating deficits in temporal acuity of Ntf3-KO mice and enhancement in Ntf3-OE mice.

Since gap-detection performance can be affected by the spectrum of the background sound (38), we assessed gap inhibition using different frequency bands (6–10 kHz, 10–14 kHz, 14–18 kHz, 22 – 26 kHz, and 38 – 42 kHz) (Fig.). As for broadband backgrounds, Ntf3-KO mice showed less inhibition of the ASR and Ntf3-OE mice showed stronger inhibition in narrowband background noise (Fig. 9B2, C2) without changing the response to the startle stimulus alone in the presence of the continuous background (Fig. 9B1, C1).

Discussion

The auditory central nervous system is comprised of several parallel pathways. This division of labor in the analysis of auditory signals begins in the cochlear nucleus, where the central axons of auditory nerve fibers branch to innervate numerous distinct cell types. The sensory limb of the acoustic startle reflex in rodents comprises one of these parallel pathways. It is driven by auditory-nerve activation of a subset of its targets, known as the cochlear root neurons. Cochlear root neurons, in turn, project to a region of the midbrain, the caudal pontine reticular nucleus, which ultimately excites the spinal motor neurons that elicit the whole-body startles measured here (39, 40). Lesion studies suggest that other regions of the cochlear nucleus can also modulate the strength of the startle (41, 42) and that pre-pulse inhibition of the acoustic startle is dominated by input from the inferior colliculus (43). Indeed, electrophysiological

measures of gap detection in inferior colliculus neurons in mice compare well with data from mouse GPIAS studies (44).

In humans with sensorineural hearing loss, longer gap detection thresholds correlate with poorer speech perception (45-47). Our results show that gap-detection is diminished with synaptopathy and improved with supranormal IHC synapse density, thus supporting the notion that noise- and age-induced synaptopathy (3, 11, 15) contribute to the deficits in auditory processing seen in humans.

Since the Plp1-CreERT transgene also drives gene recombination in oligodendrocytes (26), it was important to determine if the mice had significant changes in Ntf3 expression and signaling in the central nervous system. The finding of little or no change in Ntf3 and VGF expression in the cortex of Ntf3 KO and OE mice, together with the findings that few CNS neurons express the Ntf3 receptor TrkC in the brain (see Expression Summary in (48)) suggest that the Ntf3 manipulations we created did not directly affect cortical circuits. Thus, the phenotypes seen here are likely dominated by changes originating with the cochlear synaptic hyperplasia or dysplasia.

Analysis of ABR waveforms in our mouse models provides insight into the impact of IHC synapse density on the function of the ascending auditory pathway. As seen in animals with noise-induced or age-related synaptopathy (3, 11), later ABR peaks after Ntf3 knockdown were normal despite reduced P1 amplitude, and fewer IHC synapses. These observations suggest that homeostatic compensation in the auditory brainstem and midbrain occurs independent of mechanisms driving the cochlear synaptopathy, at least with respect to the neuronal circuits dominating the ABR response. Indeed, loss of IHC-SGN synapses results in increased central response gain in auditory circuits (49), including in the inferior colliculus and cortex (12, 13).

Interestingly, the Ntf3 knockdown mice did not show enhancement of the magnitude of the baseline acoustic startle, or of the PPI of acoustic startle, which has been observed in both noise-induced (11) and age-related (50) hearing loss in mice. This hyper-responsiveness has been interpreted as a sign of hyperacusis, a clinical disorder associated with noise-induced or age-related hearing loss, in which moderate-intensity sounds become intolerably loud (23, 50-53). There are several ways to view this apparent discrepancy. First, given the parallel processing inherent in the organization of the auditory brainstem and midbrain, it is not surprising that the adjustments in excitation/inhibition balance in the bushy-cell circuits driving the ABR could be different from those in the root cell circuit driving the acoustic startle. Secondly, it may be significant that the synapse reduction in the present experiment occurred during the neonatal period, when central circuits are still developing, whereas the synaptopathy in the noise-damage and aging studies was introduced after the circuits were fully formed. Thirdly, the present results may differ from those in prior studies of noise- or drug- or age-related synaptopathy because the synaptic loss here (20–30%) was less than that seen in other studies (40–80%). Fourthly, in noise-induced synaptopathy, the hyper-responsiveness was strongest when the startle was measured in the presence of background noise, and in the present study background noise was not added.

The amplitudes of ABR peaks I through IV were increased in mice with Ntf3 overexpression, suggesting that auditory function can be enhanced to supranormal levels by increasing IHC synapse density. In prior work, we showed that Ntf3-induced increase in synaptic counts is not associated with a proliferation of auditory nerve fibers (19). Thus, we assume that a fraction of fibers now must make more than just one synaptic contact with an IHC. This, in turn, might lead to better synchronization of onset responses and higher ABR amplitudes, which are then propagated through the ascending central circuitry. We observed that Ntf3 overexpression improved the detectability of noise gaps, suggesting it might also improve auditory performance in a wider range of stimulus contexts.

In summary, our finding that cochlear synaptopathy, elicited without cochlear insult such as noise or ototoxic drugs, results in temporal processing deficits further supports the notion that synaptopathy is a key contributor to the impaired speech perception experienced by many with hidden hearing loss. Furthermore, the improvement in temporal acuity achieved by increasing Ntf3 expression and synapse density suggests a therapeutic strategy for improving hearing in noise for individuals with synaptopathy of various etiologies.

Materials and methods

Animals

All experimental procedures complied with the National Institutes of Health guidelines and were approved by the Institutional Animal Care and Use Committee of University of Michigan, MI, USA. Cochlear supporting-cell specific Ntf3 knockout mice (Ntf3 KO derived from *Ntf3$^{flox/flox}$:Plp1/CreER^{T}* mice by Cre-recombination) and Ntf3 overexpressing mice (Ntf3 OE derived from *Ntf3^{stop}:Plp1/CreER^{T}* mice by Cre-recombination) were generated as previously described (19). *Ntf3 KO* mice and their controls were maintained on C57BL/6 background. *Ntf3 OE* and their controls were on FVB/N background. Both male and female mice were included in this study.

Tamoxifen administration

Tamoxifen was injected into intraperitoneal cavity of P 3-10 Ntf3^{stop}: Plp1/CreER^{T} mice or P1-3 Ntf3$^{flox/flox}$:Plp1/CreER^{T} mice as previously described (19). A 10 mg/ml solution of tamoxifen was obtained by dissolution in corn oil. Injection was 33 mg/kg for Ntf3^{stop}: Plp1/CreER^{T} mice and 50 mg/kg for Ntf3$^{flox/flox}$:Plp1/CreER^{T} mice.

Distortion Product Otoacoustic Emissions (DPOAE) and Auditory Brainstem Responses (ABR)

DPOAEs and ABRs were performed as previously described (19). Mice were anaesthetized by i.p. injections of xylazine (20 mg kg^{-1}, i.p.) and ketamine (100 mg kg^{-1}, i.p.). The DPOAEs were induced by two primary tones (f1 and f2) and recorded at (2 × f1)−f2. f1 level was10 dB higher than the f2 level and frequency ratio f2/f1 was 1.2. The ear-canal sound pressure was amplified and averaged at 4 µs intervals. DPOAE thresholds were defined as the f2 level that produced a response 10 dB SPL higher than the noise floor. For ABR measurement, subdermal electrodes were placed (a) at the dorsal midline of the head, (b) behind the left earlobe and (c) at the base of the tail (for a ground electrode). ABRs were evoked with 5 ms tone pips (0.5 ms rise–fall) delivered to the eardrum. The frequencies of tone pips were 5.6, 8, 11.3, 16, 22.6, 32 and 45.2 kHz, with 15 sound levels from 10 to 80 dB SPL for each frequency. The signals were amplified 10,000 times and filtered through a 0.3 - 3 kHz passband. At each level, the average of 1,024 signals were taken after ‘artifact rejection.’ Both recordings were performed using National Instruments input/output boards hardware. Offline analysis was performed using excel and ABR peak analysis software.

PPI and gap detection/GPIAS

Mice were tested in a 10 x 4.5 x 4 cm cage inside a sound-isolation chamber that were placed within a sound attenuating room. Acoustic sound source was located in the upper part of this chamber. The piezoelectric motion sensor attached to the cage detected the vertical force of the

startle reflex. All ASR, PPI and GPIAS stimuli and responses were generated and recorded with Kinder Scientific Startle Monitor (Kinder Scientific, Poway, CA).

PPI tests were used for assessing sensorimotor gating on 9–16 old week mice, twice a week, each 2 days apart. PPI tests were conducted quiet. The startle stimuli were BBN bursts at 120 dB SPL, 20 ms in duration, 0.1 ms rise-fall times. The prepulse was a narrow band sound centered at 8, 12, 16, 24 and 40 kHz, 50 ms in duration, with 2-ms rise-fall ramps. PPI test consisted of prepulse trials and startle-only trials, which were delivered alternatively. In prepulse trials, a prepulse ended 1or 50 ms before the startle stimulus. Startle-only trials were similar to the prepulse trials, but no prepulse was delivered. PPI startle ratio is the ratio of the startle magnitude in prepulse trials over the startle magnitude in startle-only trials.

The GPIAS paradigm has been used for measuring auditory temporal processing (20, 25). Gap inhibition was assessed on 8-19 old week mice, twice a week, 2 days apart. The testing consists of two types of trials, gap trials and no-gap trials (Figure 8-9) that were delivered alternatively. In both trials, the startle stimulus was 20 ms BBN at 120 dB with 0.1 ms rise/fall times). The startle was preceded either by gaps with varied durations (3-, 5-, 15-, 25-, or 50-ms long) embedded in BBN or by a 50-ms gap embedded in a narrow bandpass background sound centered at 8, 12, 16, 24, and 40 kHz at 65 dB. For gaps with varied durations, the response was normalized to the longest gap (50 ms) on the presumption that the maximum level of inhibition (100%) was elicited at the longest gap. The responses and gap durations were fitted with three-parameter logistic regression models. The gap-detection threshold was defined as the value of the fitted curve that elicited 50% of the maximal inhibition achieved per mouse. Gap-startle ratio is the ratio of the startle magnitude in gap trials over the startle magnitude of the paired no-gap trials.

For each mouse, PPI and gap-startle ratios were averaged from 11 sessions. Each session of PPI and gap-PPI test included 60 pairs of prepulse and startle-only trials for PPI or gap and no-gap trials for gap detection (5 prepulse or background sound frequencies, 12 pairs for each frequency). The interval between trials was randomly varied between 5 and 15s. Each session began with a 2-min acclimatization period in the cage before startle testing began, and all tests were conducted in darkness. Startle-only trials and no-gap trial amplitudes greater than or equal to mean ± 2.5 standard deviations were eliminated. When a trial was eliminated, its paired trial was also eliminated. PPI ratio bigger than 1 or gap-startle ratios bigger than 1.1 were excluded (54). PPI and gap-startle ratios were calculated as the average with prepulse startle amplitude divided by the mean without prepulse startle amplitude.

Real-time quantitative RT-PCR.

Total RNA was isolated from the cortical brain and cochlea samples from 1-month-old mice using RNA extraction kit and Qiazol Reagent (RNeasy mini kit; Qiagen, Germany), and DNase treatment was performed (RNase-free; Qiagen). The complementary DNA was synthesized using iScript cDNA synthesis kit (Bio-Rad, #1708891, USA), according to the manufacturers' protocol. Quantitative RT-PCR was performed on a CFX-96 Bio-Rad reverse transcription polymerase chain reaction detection system (Hercules, CA, USA) using iTaq Universal SYBR® Green supermix (Bio-Rad, # 172-5121, USA) and primer pairs were synthesized by IDT (Coralville, IA, USA). All samples and standard curves were run in triplicate. Water instead of complementary DNA was used as a negative control. The 10 µl reaction contained 5 µl of SYBR Green supermix, 6 pmol of each forward and reverse primer (0.6 µl), 1.9 µl nuclease-free of water and 2.5 µl of cDNA sample. The mRNA expression levels in PLP1cre ERT: NT3fl or PLP1cre ERT: NT3 STOP versus their control mice were determined by a comparative cycle threshold (Ct) method and relative gene copy number was calculated as normalized gene expression, defined as described previously (55). Ribosomal protein L19 (RPL19) was used as the housekeeping gene. The following specific oligo primers were used for the target genes:

Rpl19, F: 5'ACCTGGATGAGAAGGATGAG 3'; R: 5'ACCTTCAGGTACAGGCTGTG 3'; Ntf3, F 5'GCCCCCTCCCTTATACCTAATG 3'; R: 5'CATAGCGTTTCCTCCGTGGT 3'; Vgf: 'F 5'GGTAGCTGAGGACGCAGTGT 3'; R: 5'GTCCAGTGCCTGCAACAGT 3'. Changes in mRNA expression were calculated as relative expression (arbitrary units) respective to the control group for each mouse line.

Immunostaining and synaptic counts

Cochleas from 16-week-old mice were prepared for whole-mount imaging as described in (19). In brief, the samples were fixed with 4% formaldehyde for 2 hours and then decalcified with 5% ethylenediaminetetraacetic acid (EDTA) for 3-5 days. Cochlear epithelia were micro-dissected into five segments for whole mount processing. The cochlea segments were incubated with 30% sucrose for 1 hour for permeabilization and then blocked with 5% normal horse serum for 1 hour. Afterwards, the following primary antibodies were used: 1) CtBP2 to visualize synaptic ribbons (mouse anti-CtBP2 at 1:200, BD Biosciences, catalog # 612044, RRID: AB_399431), 2) GluR2 to visualize postsynaptic receptors (mouse anti-GluR2 at 1:2000, Millipore, catalog # MAB397, RRID: AB_2113875) and 3) Myosin VIIa to visualize IHCs (rabbit anti-Myosin VIIa at 1:200; Proteus Biosciences, catalog # 25-6790, RRID: AB_10015251). Secondary antibodies used were Alexa Fluor 488 conjugated anti-mouse IgG2a (1:1000, Invitrogen), Alexa Fluor 568 conjugated anti-mouse IgG1 (1:1000, Invitrogen) and Alexa Fluor 647 conjugated anti-rabbit (1:1000, Life Technologies). Frequency maps were created using a custom ImageJ plug-in. Images were captured from 5.6 to 45.2 kHz using a Leica SP8 with a 1.4 NA 63x oil immersion objective at 3 digital zoom. Offline image analysis was performed using Amira (Visage Imaging). Quantifications of synapses were done by a blind investigator.

Statistical analyses

Data were analyzed using Graphpad Prism 6 (Graphpad Software Inc., La Jolla, CA) and Rstudio packages. Data are shown as mean and standard error of the mean (S.E.M.). The number of replicates (n) is indicated in the results section and figure legends. No explicit power analysis was used to predetermine sample sizes, but our sample sizes are similar to those reported in our previous publications. Statistical differences in auditory physiology (DPOAE threshold, ABR threshold, amplitude, and latency), ribbon synapse counts, behavioral background movement, PPI ratio, gap-startle ratios were analyzed using two-way ANOVA, followed by Bonferroni multiple comparisons test. mRNA expression, ASR amplitude and gap detection threshold were compared using unpaired Student's *t*-test. Correlations were computed using Pearson's correlation. Statistical threshold was set to alpha = 0.05.

Figure 1

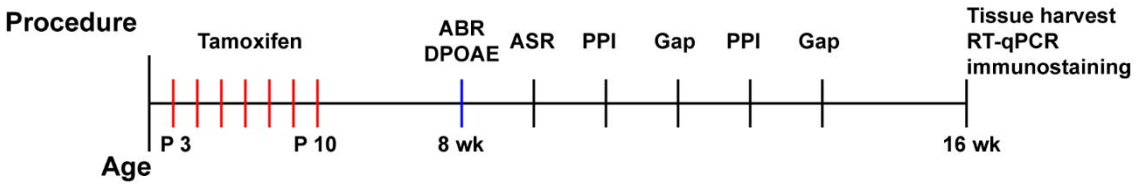
Procedure
Tamoxifen
ABR
DPOAE
ASR
PPI
Gap
PPI
Gap
Tissue harvest
RT-qPCR
immunostaining
P 3
P 10
8 wk
16 wk
Age

Figure 2

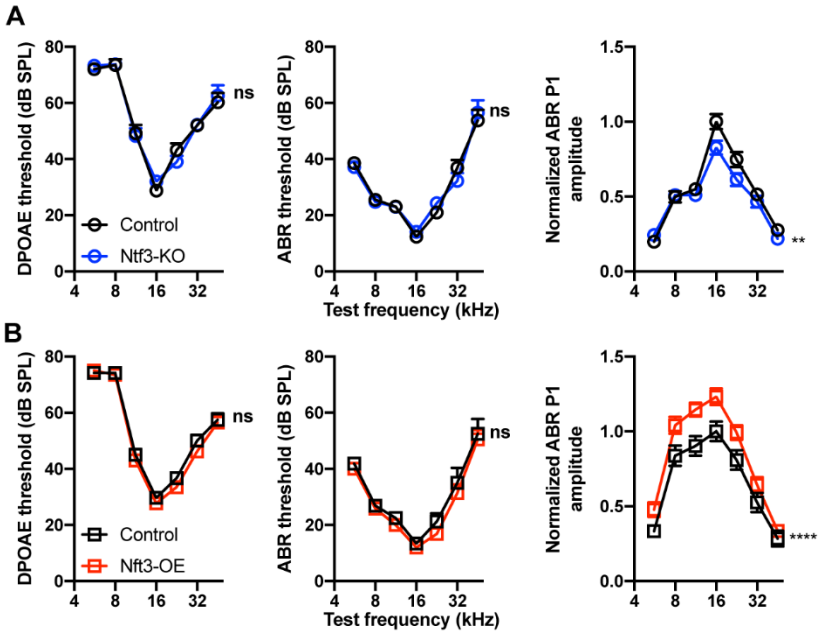
A
DPOAE threshold (dB SPL)
ns
Control
Ntf3-KO
ABR threshold (dB SPL)
ns
Test frequency (kHz)
Normalized ABR P1 amplitude
**
B
DPOAE threshold (dB SPL)
ns
Control
Nft3-OE
ABR threshold (dB SPL)
ns
Test frequency (kHz)
Normalized ABR P1 amplitude
****

Figure 3

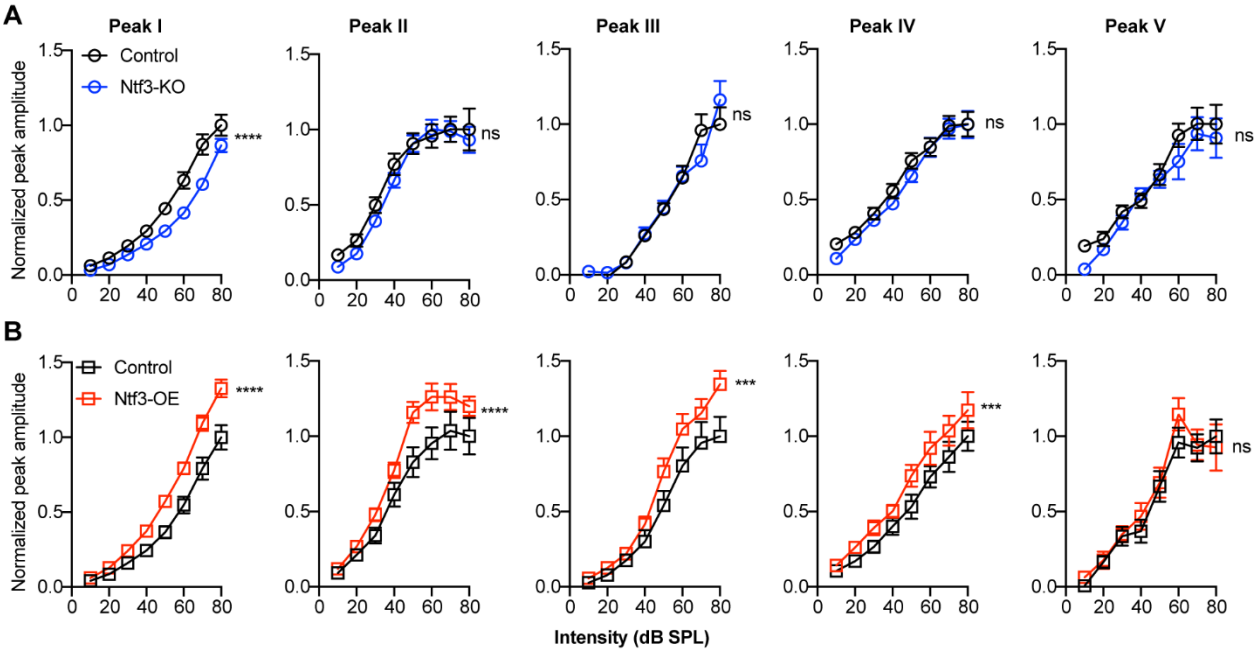
A
Peak I
Peak II
Peak III
Peak IV
Peak V
Control
Ntf3-KO
Normalized peak amplitude
****
ns
ns
ns
ns
B
Control
Ntf3-OE
Normalized peak amplitude
****
****
***
***
ns
Intensity (dB SPL)

Figure 4

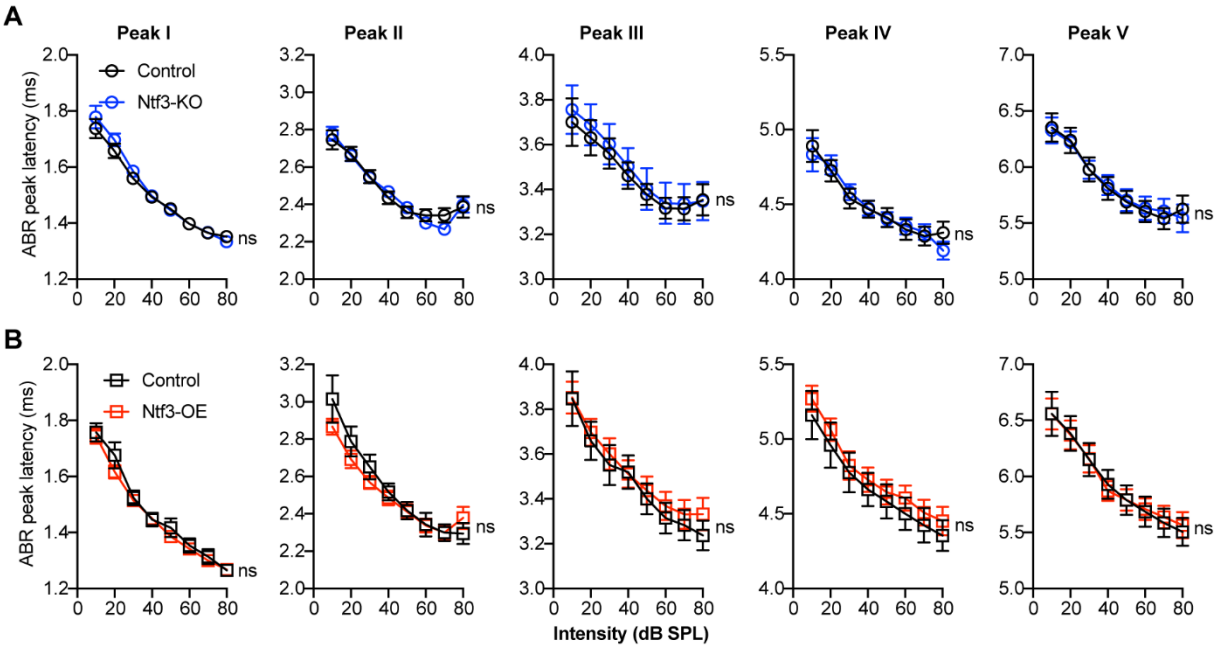
A
Peak I
Peak II
Peak III
Peak IV
Peak V
Control
Ntf3-KO
ABR peak latency (ms)
ns
B
Control
Ntf3-OE
ABR peak latency (ms)
ns
Intensity (dB SPL)

Figure 5

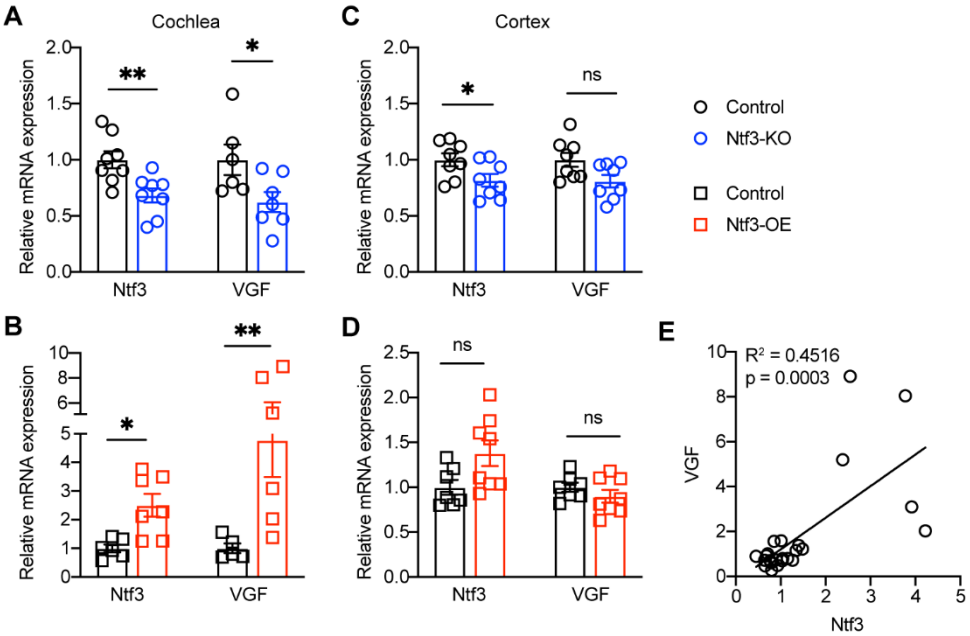
A
Cochlea
Relative mRNA expression
2.0
1.5
1.0
0.5
0.0
**
*
Ntf3
VGF
C
Cortex
*
ns
Control
Ntf3-KO
Control
Ntf3-OE
B
10
8
6
5
4
3
2
1
0
*
**
D
2.5
ns
ns
E
R² = 0.4516
p = 0.0003
VGF
Ntf3
0
1
2
3
4
5

Figure 6

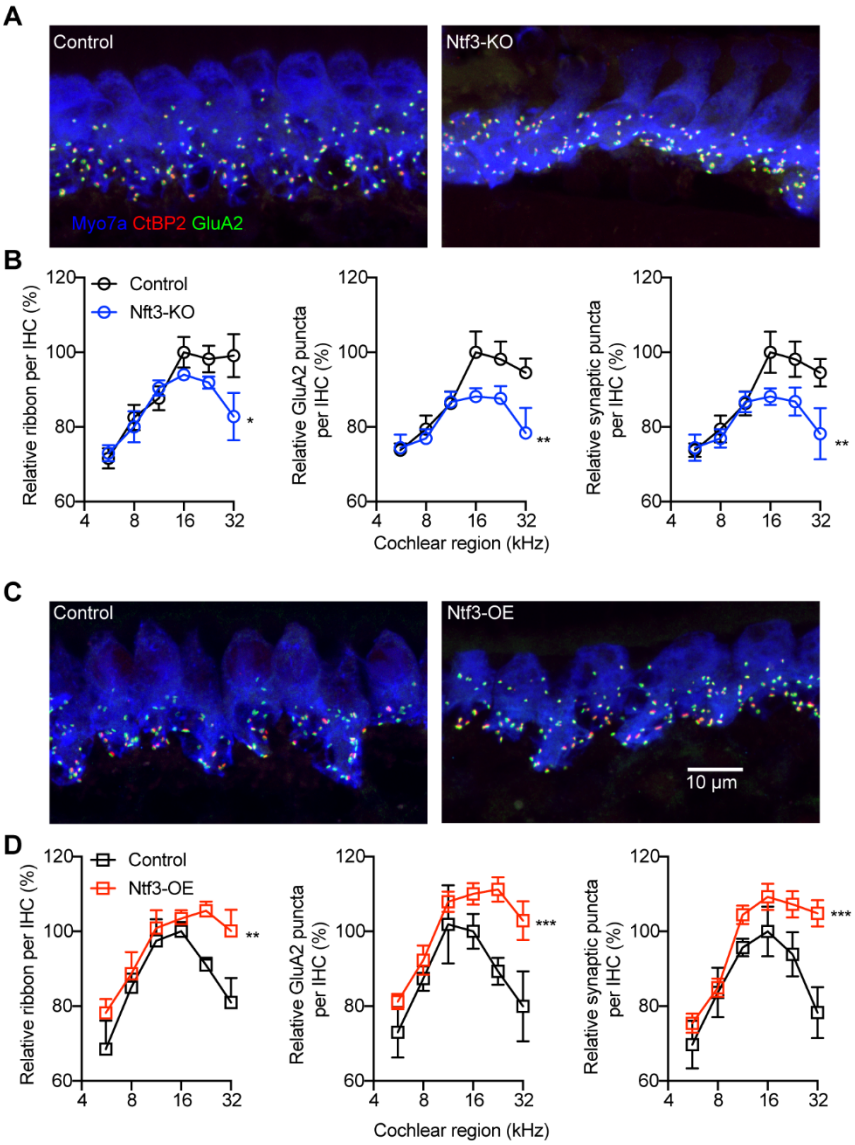
A
Control
Ntf3-KO
Myo7a CtBP2 GluA2
B
Control
Nft3-KO
Relative ribbon per IHC (%)
Relative GluA2 puncta per IHC (%)
Relative synaptic puncta per IHC (%)
Cochlear region (kHz)
C
Control
Ntf3-OE
10 µm
D
Control
Ntf3-OE
Relative ribbon per IHC (%)
Relative GluA2 puncta per IHC (%)
Relative synaptic puncta per IHC (%)
Cochlear region (kHz)

Figure 7

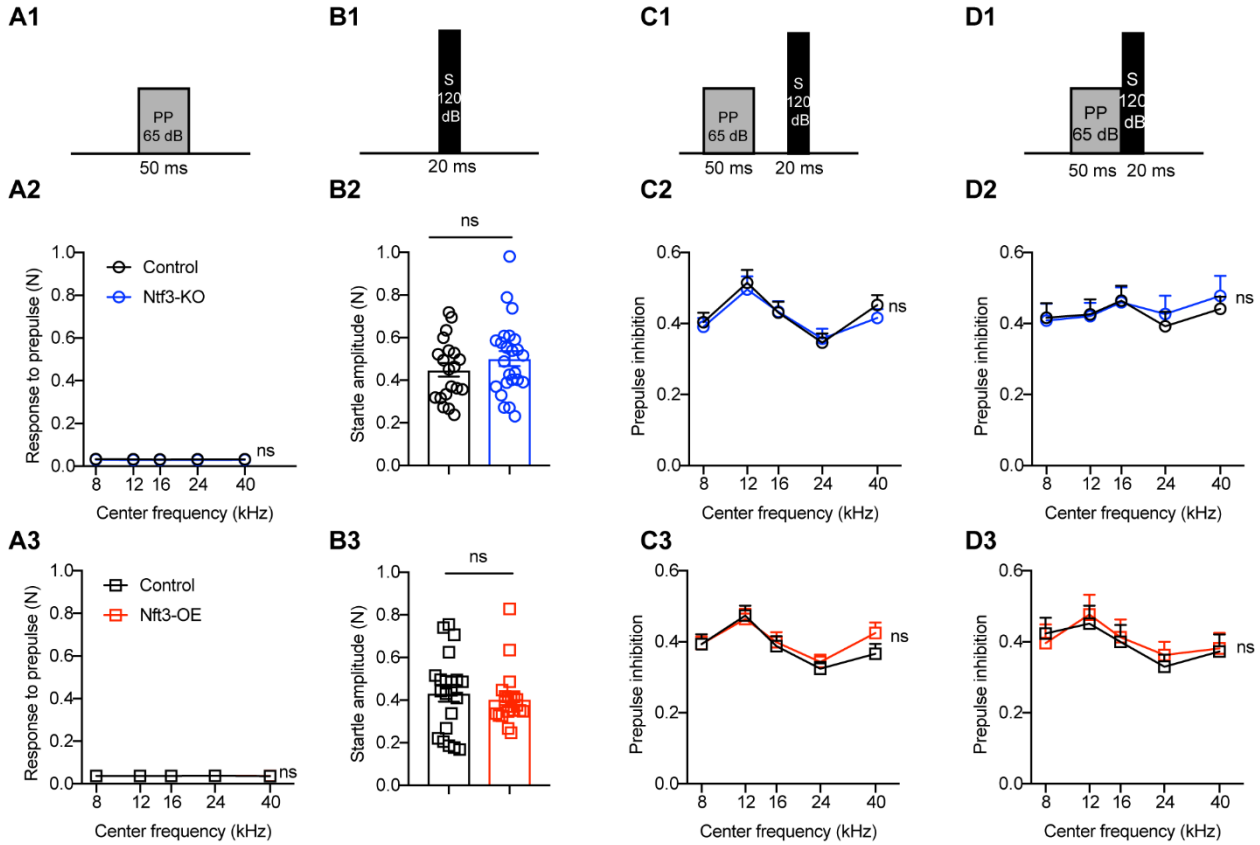
A1
PP
65 dB
50 ms
B1
S
120
dB
20 ms
C1
PP
65 dB
S
120
dB
50 ms
20 ms
D1
PP
65 dB
S
120
dB
50 ms
20 ms
A2
Control
Ntf3-KO
Response to prepulse (N)
ns
Center frequency (kHz)
B2
ns
Startle amplitude (N)
C2
Prepulse inhibition
ns
Center frequency (kHz)
D2
Prepulse inhibition
ns
Center frequency (kHz)
A3
Control
Nft3-OE
Response to prepulse (N)
ns
Center frequency (kHz)
B3
ns
Startle amplitude (N)
C3
Prepulse inhibition
ns
Center frequency (kHz)
D3
Prepulse inhibition
ns
Center frequency (kHz)

Figure 8

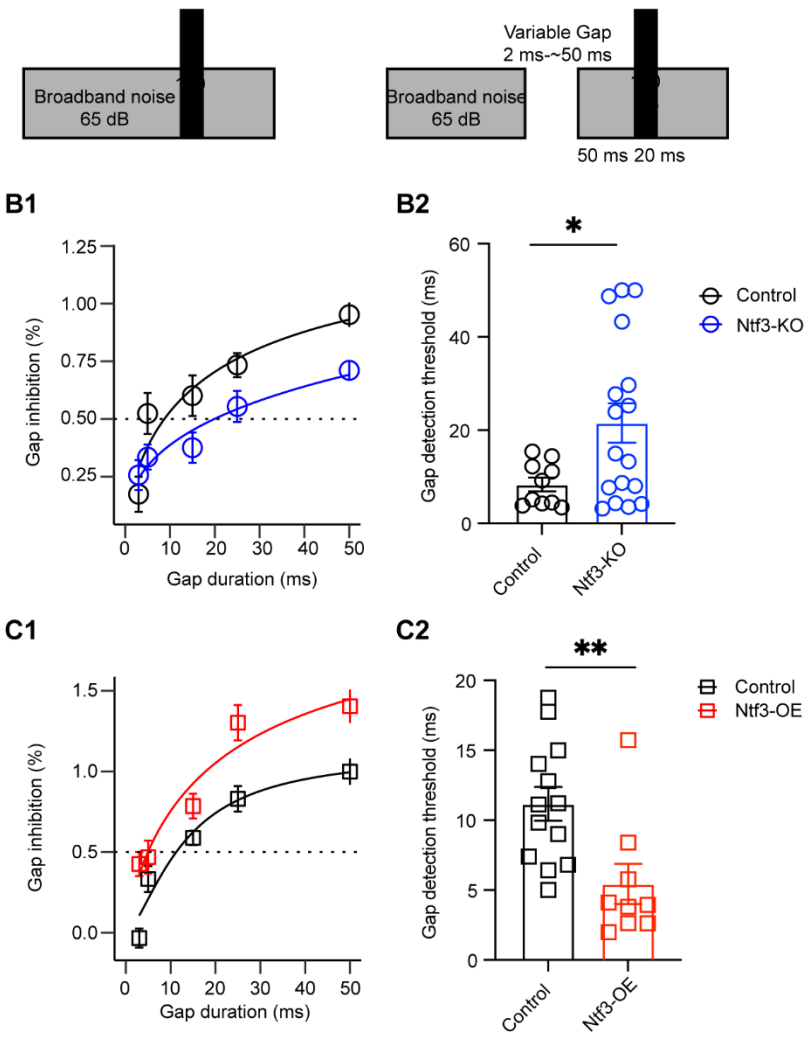
A
Broadband noise
65 dB
Variable Gap
2 ms-~50 ms
Broadband noise
65 dB
50 ms 20 ms
B1
Gap inhibition (%)
Gap duration (ms)
B2
Gap detection threshold (ms)
Control
Ntf3-KO
C1
Gap inhibition (%)
Gap duration (ms)
C2
Gap detection threshold (ms)
Control
Ntf3-OE

Figure 9

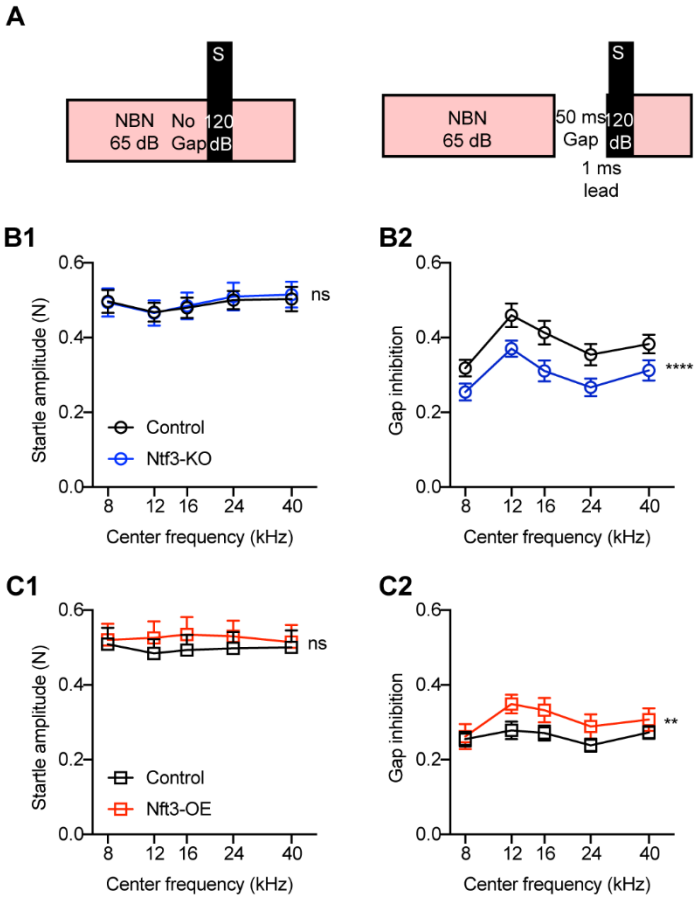
A
S
NBN
65 dB
No
Gap
120
dB
S
NBN
65 dB
50 ms
Gap
120
dB
1 ms
lead
B1
Startle amplitude (N)
0.6
0.4
0.2
0.0
ns
Control
Ntf3-KO
8
12
16
24
40
Center frequency (kHz)
B2
Gap inhibition
0.6
0.4
0.2
0.0
****
8
12
16
24
40
Center frequency (kHz)
C1
Startle amplitude (N)
0.6
0.4
0.2
0.0
ns
Control
Nft3-OE
8
12
16
24
40
Center frequency (kHz)
C2
Gap inhibition
0.6
0.4
0.2
0.0
**
8
12
16
24
40
Center frequency (kHz)

Figure legends

Figure 1. **Timeline of the experimental design.** Timeline showing the ages of mice for tamoxifen inductions (Tmx), ABR measurements, auditory behavioral assay (ASR, PPI, Gap), and sample collections for qPCR and immunostaining.

Figure 2. Ntf3 knockdown or overexpression changes ABR peak I amplitudes without effects on cochlear thresholds. Mean data (± SEM) for Ntf3-KO (**A**) and Ntf3-OE (**B**) mice compared to their respective controls. *n* = 15-24. Normalized ABR P1 amplitudes were assessed at 80 dB SPL. Ns, $p > 0.05$, *$p < 0.05$, **$p < 0.01$, ***$p < 0.001$, ***$p < 0.0001$ by two-way ANOVA.

Figure 3. Ntf3 knockdown or overexpression modulates ABR growth functions. Mean amplitude-vs level functions (± SEM) for ABR peaks I-IV in Ntf3-KO (**A**) and Ntf3-OE (B) mice compared to their respective controls at 16 kHz. n=14-20, ns, $p > 0.05$, *$p < 0.05$, **$p < 0.01$, ***$p < 0.001$, ***$p < 0.0001$ by two-way ANOVA.

Figure 4. Ntf3 knockdown or overexpression has no effect on ABR peak latencies. Mean ABR wave I-IV latencies (± SEM) recorded at 16 kHz are normal in Ntf3-KO (**A**) and Ntf3-OE (**B**) mice. n=14-20, ns, $p > 0.05$ by two-way ANOVA.

Figure 5. Ntf3 expression levels impact TrkC signaling in the cochlea, but not in the CNS. mRNA level of Ntf3 and a downstream gene, VGF, are reduced in Ntf3-KO cochleas (**A**) and increased in Ntf3-OE cochleas (B). In contrast, cortical Ntf3 mRNA is slightly decreased in Ntf3-KOs (**C**) and unchanged in Ntf3-OEs (**D**). No changes in VGF mRNA levels are observed in either Ntf3-KO or Ntf3-OE mice (**C** and **D**). (**E**) Correlation between cochlear levels of Ntf3 and VGF. n=5-8, ns, $p > 0.05$, *$p < 0.05$, **$p < 0.01$, mRNA levels were compared by two-tailed unpaired t test.

Figure 6. Ntf3 expression regulates IHC synapse density. Representative confocal images of IHC synapses in Ntf3-KO and Ntf3-OE cochleas immunolabeled for pre-synaptic ribbons (CtBP2 - red), post-synaptic receptor patches (GluA2 - green) and hair cells (Myo7a - blue) (**A** and **C**). Mean counts (± SEM) of ribbons, GluA2 patches and colocalized markers in Ntf3 KOs and OEs (**B** and **D**). n = 5, ns, $p > 0.05$, *$p < 0.05$, **$p < 0.01$, ***$p < 0.001$, ***$p < 0.0001$. synaptic markers were compared by two-way ANOVA.

Figure 7. IHC synapse density does not influence the acoustic startle response or prepulse inhibition. Schematics of the protocols for prepulse alone (**A1**), startle stimulus alone (**B1**), prepulse and startle stimuli with long lead interval (50 ms, **C1**), and prepulse and startle stimuli with short lead interval (1 ms, **D1**). Reduced (**A2-D2**) or increased (**A3-D3**) Ntf3 expression and IHC synapse density do not alter responses to a startle stimulus or pre-pulse inhibition. Mean ± SEM are shown. For response to prepulse (**A2, A3**), n=18-20 mice/group; for startle response (**B2, B3**), n=20-24 mice/group; for PPI at 50 ms lead time, 15-20 mice/ group; for PPI at 1 ms lead time, 9-17 mice/ group. ns, $p > 0.05$ by two-tailed unpaired t tests (**B2, B3**) or two-way ANOVA.

Figure 8. Gap detection thresholds in broadband noise are influenced by Ntf3 expression levels. (**A**) Schematic of the protocols showing the startle alone in continuous broadband noise (left) and the startle preceded by a silent gap (right) of varying lengths ending 50 ms before the startle stimulus. (**B1, C1**) The level of gap inhibition vs. gap length for Ntf3 KO and OE mice,

respectively. Dotted line: threshold defined at 50% inhibition used in B2, C2. (**B2, C2**) Gap-detection threshold is increased in Ntf3-KO and decreased in Ntf3-OE mice. n=9-17 mice/group, mean ± SEM are shown. *p < 0.05, **p < 0.01 by t-test.

Figure 9. Gap detection thresholds in narrowband noise are influenced by Ntf3 expression levels. (**A**) Schematic of the protocols showing startle alone in continuous narrowband noise (left) and startle with a preceding 50 ms noise gap (right) ending 1 ms before startle onset. (**B1, C1**) Responses to startle only in narrowband noise are unaffected. (**B2, C2**) GPIAS in narrowband noises were weakened in Ntf3-KO mice and strengthened in Ntf3-OE mice. n=10-15 mice/group, mean ± SEM are shown. *p < 0.05, **p < 0.01 by two-way ANOVA.

References

1. Kujawa SG, Liberman MC. Synaptopathy in the noise-exposed and aging cochlea: Primary neural degeneration in acquired sensorineural hearing loss. Hearing Research. 2015;330:191-9. doi: 10.1016/j.heares.2015.02.009.

2. Kujawa SG, Liberman MC. Adding Insult to Injury: Cochlear Nerve Degeneration after “Temporary” Noise-Induced Hearing Loss. J Neurosci. 2009;29(45):14077-85. doi: 10.1523/JNEUROSCI.2845-09.2009.

3. Sergeyenko Y, Lall K, Liberman MC, Kujawa SG. Age-Related Cochlear Synaptopathy: An Early-Onset Contributor to Auditory Functional Decline. J Neurosci. 2013;33(34):13686-94. doi: 10.1523/JNEUROSCI.1783-13.2013.

4. Lin HW, Furman AC, Kujawa SG, Liberman MC. Primary Neural Degeneration in the Guinea Pig Cochlea After Reversible Noise-Induced Threshold Shift. J Assoc Res Otolaryngol. 2011;12(5):605-16. doi: 10.1007/s10162-011-0277-0.

5. Möhrle D, Ni K, Varakina K, Bing D, Lee SC, Zimmermann U, Knipper M, Rüttiger L. Loss of auditory sensitivity from inner hair cell synaptopathy can be centrally compensated in the young but not old brain. Neurobiology of Aging. 2016;44:173-84. doi: 10.1016/j.neurobiolaging.2016.05.001.

6. Gleich O, Semmler P, Strutz J. Behavioral auditory thresholds and loss of ribbon synapses at inner hair cells in aged gerbils. Experimental Gerontology. 2016;84:61-70. doi: 10.1016/j.exger.2016.08.011.

7. Hickman TT, Smalt C, Bobrow J, Quatieri T, Liberman MC. Blast-induced cochlear synaptopathy in chinchillas. Scientific Reports. 2018;8(1):10740. doi: 10.1038/s41598-018-28924-7.

8. Viana LM, O’Malley JT, Burgess BJ, Jones DD, Oliveira CACP, Santos F, Merchant SN, Liberman LD, Liberman MC. Cochlear neuropathy in human presbycusis: confocal analysis of hidden hearing loss in post-mortem tissue. Hearing Research. 2015;327:78-88. doi: 10.1016/j.heares.2015.04.014.

9. Wu PZ, Liberman LD, Bennett K, de Gruttola V, O’Malley JT, Liberman MC. Primary neural degeneration in the human cochlea: evidence for hidden hearing loss in the aging ear. Neuroscience. 2019;407:8-20. doi: 10.1016/j.neuroscience.2018.07.053.

10. Liberman MC, Kujawa SG. Cochlear synaptopathy in acquired sensorineural hearing loss: Manifestations and mechanisms. Hearing Research. 2017;349:138-47. doi: 10.1016/j.heares.2017.01.003.

11. Hickox AE, Liberman MC. Is noise-induced cochlear neuropathy key to the generation of hyperacusis or tinnitus? Journal of Neurophysiology. 2014;111(3):552-64. doi: 10.1152/jn.00184.2013.

12. Asokan MM, Williamson RS, Hancock KE, Polley DB. Sensory overamplification in layer 5 auditory corticofugal projection neurons following cochlear nerve synaptic damage. Nat Commun. 2018;9(1):2468. Epub 2018/06/27. doi: 10.1038/s41467-018-04852-y. PubMed PMID: 29941910; PMCID: PMC6018400.

13. Resnik J, Polley DB. Cochlear neural degeneration disrupts hearing in background noise by increasing auditory cortex internal noise. Neuron. 2021;109(6):984-96 e4. Epub 2021/02/10. doi: 10.1016/j.neuron.2021.01.015. PubMed PMID: 33561398; PMCID: PMC7979519.

14. Chen H, Xing Y, Zhang Z, Tao S, Wang H, Aiken S, Yin S, Yu D, Wang J. Coding-in-Noise Deficits are Not Seen in Responses to Amplitude Modulation in Subjects with cochlear Synaptopathy Induced by a Single Noise Exposure. Neuroscience. 2019;400:62-71. Epub 2019/01/08. doi: 10.1016/j.neuroscience.2018.12.048. PubMed PMID: 30615912.

15. Liberman MC, Epstein MJ, Cleveland SS, Wang H, Maison SF. Toward a Differential Diagnosis of Hidden Hearing Loss in Humans. PLOS ONE. 2016;11(9):e0162726. doi: 10.1371/journal.pone.0162726.

16. Bramhall N, Ong B, Ko J, Parker M. Speech Perception Ability in Noise is Correlated with Auditory Brainstem Response Wave I Amplitude. J Am Acad Audiol. 2015;26(5):509-17. doi: 10.3766/jaaa.14100.

17. Grant KJ, Mepani AM, Wu P, Hancock KE, de Gruttola V, Liberman MC, Maison SF. Electrophysiological markers of cochlear function correlate with hearing-in-noise performance among audiometrically normal subjects. J Neurophysiol. 2020;124(2):418-31. Epub 2020/07/09. doi: 10.1152/jn.00016.2020. PubMed PMID: 32639924; PMCID: PMC7500376.

18. Guest H, Munro KJ, Prendergast G, Millman RE, Plack CJ. Impaired speech perception in noise with a normal audiogram: No evidence for cochlear synaptopathy and no relation to lifetime noise exposure. Hearing Research. 2018;364:142-51. doi: 10.1016/j.heares.2018.03.008.

19. Wan G, Gómez-Casati ME, Gigliello AR, Liberman MC, Corfas G. Neurotrophin-3 regulates ribbon synapse density in the cochlea and induces synapse regeneration after acoustic trauma. Elife. 2014;3. doi: 10.7554/eLife.03564.

20. Fournier P, Hebert S. The gap prepulse inhibition of the acoustic startle (GPIAS) paradigm to assess auditory temporal processing: Monaural versus binaural presentation. Psychophysiology. 2021;58(3):e13755. Epub 2020/12/29. doi: 10.1111/psyp.13755. PubMed PMID: 33355931.

21. Jafari Z, Kolb BE, Mohajerani MH. Prepulse inhibition of the acoustic startle reflex and P50 gating in aging and alzheimer's disease. Ageing Res Rev. 2020;59:101028. Epub 2020/02/25. doi: 10.1016/j.arr.2020.101028. PubMed PMID: 32092463.

22. Moore S, Meschkat M, Ruhwedel T, Trevisiol A, Tzvetanova ID, Battefeld A, Kusch K, Kole MHP, Strenzke N, Mobius W, de Hoz L, Nave KA. A role of oligodendrocytes in information processing. Nat Commun. 2020;11(1):5497. Epub 2020/11/01. doi: 10.1038/s41467-020-19152-7. PubMed PMID: 33127910; PMCID: PMC7599337.

23. Thomas ME, Guercio GD, Drudik KM, de Villers-Sidani É. Evidence of Hyperacusis in Adult Rats Following Non-traumatic Sound Exposure. Front Syst Neurosci. 2019;13:55. doi: 10.3389/fnsys.2019.00055.

24. Salloum RH, Yurosko C, Santiago L, Sandridge SA, Kaltenbach JA. Induction of enhanced acoustic startle response by noise exposure: dependence on exposure conditions

and testing parameters and possible relevance to hyperacusis. PLOS ONE. 2014;9(10):e111747. Epub 2014/11/02. doi: 10.1371/journal.pone.0111747. PubMed PMID: 25360877; PMCID: PMC4216136.

25. Turner JG, Brozoski TJ, Bauer CA, Parrish JL, Myers K, Hughes LF, Caspary DM. Gap detection deficits in rats with tinnitus: A potential novel screening tool. Behavioral Neuroscience. 2006;120(1):188-95. doi: 10.1037/0735-7044.120.1.188.

26. Doerflinger NH, Macklin WB, Popko B. Inducible site-specific recombination in myelinating cells. genesis. 2003;35(1):63-72. doi: 10.1002/gene.10154.

27. Gómez-Casati ME, Murtie J, Taylor B, Corfas G. Cell-Specific Inducible Gene Recombination in Postnatal Inner Ear Supporting Cells and Glia. JARO. 2010;11(1):19-26. doi: 10.1007/s10162-009-0191-x.

28. Eagleson KL, Fairfull LD, Salton SR, Levitt P. Regional differences in neurotrophin availability regulate selective expression of VGF in the developing limbic cortex. J Neurosci. 2001;21(23):9315-24. Epub 2001/11/22. PubMed PMID: 11717365; PMCID: PMC6763919.

29. Buchwald JS, Huang C. Far-field acoustic response: origins in the cat. Science. 1975;189(4200):382-4. doi: 10.1126/science.1145206.

30. Melcher JR, Guinan JJ, Knudson IM, Kiang NYS. Generators of the brainstem auditory evoked potential in cat. II. Correlating lesion sites with waveform changes. Hearing Research. 1996;93(1):28-51. doi: 10.1016/0378-5955(95)00179-4.

31. Melcher JR, Kiang NYS. Generators of the brainstem auditory evoked potential in cat III: identified cell populations. Hearing Research. 1996;93(1):52-71. doi: 10.1016/0378-5955(95)00200-6.

32. Melcher JR, Knudson IM, Fullerton BC, Guinan JJ, Norris BE, Kiang NYS. Generators of the brainstem auditory evoked potential in cat. I. An experimental approach to their identification. Hearing Research. 1996;93(1):1-27. doi: 10.1016/0378-5955(95)00178-6.

33. Starr A, Hamilton AE. Correlation between confirmed sites of neurological lesions and abnormalities of far-field auditory brainstem responses. Electroencephalography and clinical neurophysiology. 1976;41(6):595-608. doi: 10.1016/0013-4694(76)90005-5.

34. Curzon P, Zhang M, Radek RJ, Fox GB. The Behavioral Assessment of Sensorimotor Processes in the Mouse: Acoustic Startle, Sensory Gating, Locomotor Activity, Rotarod, and Beam Walking. In: Buccafusco JJ, editor. Methods of Behavior Analysis in Neuroscience. 2nd ed. Boca Raton (FL): CRC Press/Taylor & Francis; 2009.

35. Felix RA, 2nd, Chavez VA, Novicio DM, Morley BJ, Portfors CV. Nicotinic acetylcholine receptor subunit alpha7-knockout mice exhibit degraded auditory temporal processing. J Neurophysiol. 2019;122(2):451-65. Epub 2019/05/23. doi: 10.1152/jn.00170.2019. PubMed PMID: 31116647; PMCID: PMC6734398.

36. Heeke P, Vermiglio AJ, Bulla E, Velappan K, Fang X. The Relationship between Random Gap Detection and Hearing in Noise Test Performances. J Am Acad Audiol. 2018;29(10):948-54. Epub 2018/11/28. doi: 10.3766/jaaa.18005. PubMed PMID: 30479267.

37. Nakajima Y, Matsuda M, Ueda K, Remijn GB. Temporal Resolution Needed for Auditory Communication: Measurement With Mosaic Speech. Front Hum Neurosci. 2018;12:149. Epub 2018/05/10. doi: 10.3389/fnhum.2018.00149. PubMed PMID: 29740295; PMCID: PMC5928238.

38. Ison JR, Allen PD, Rivoli PJ, Moore JT. The behavioral response of mice to gaps in noise depends on its spectral components and its bandwidth. J Acoust Soc Am. 2005;117(6):3944-51. Epub 2005/07/16. doi: 10.1121/1.1904387. PubMed PMID: 16018496.

39. Lee Y, Lopez DE, Meloni EG, Davis M. A primary acoustic startle pathway: obligatory role of cochlear root neurons and the nucleus reticularis pontis caudalis. J Neurosci. 1996;16(11):3775-89. Epub 1996/06/01. PubMed PMID: 8642420; PMCID: PMC6578836.

40. Lingenhohl K, Friauf E. Giant neurons in the rat reticular formation: a sensorimotor interface in the elementary acoustic startle circuit? J Neurosci. 1994;14(3 Pt 1):1176-94. Epub 1994/03/01. PubMed PMID: 8120618; PMCID: PMC6577542.

41. Meloni EG, Davis M. The dorsal cochlear nucleus contributes to a high intensity component of the acoustic startle reflex in rats. Hear Res. 1998;119(1-2):69-80. Epub 1998/06/26. doi: 10.1016/s0378-5955(98)00040-9. PubMed PMID: 9641320.

42. Yeomans JS, Frankland PW. The acoustic startle reflex: neurons and connections. Brain Res Brain Res Rev. 1995;21(3):301-14. Epub 1995/11/01. doi: 10.1016/0165-0173(96)00004-5. PubMed PMID: 8806018.

43. Fendt M, Li L, Yeomans JS. Brain stem circuits mediating prepulse inhibition of the startle reflex. Psychopharmacology (Berl). 2001;156(2-3):216-24. Epub 2001/09/11. doi: 10.1007/s002130100794. PubMed PMID: 11549224.

44. Barsz K, Ison JR, Snell KB, Walton JP. Behavioral and neural measures of auditory temporal acuity in aging humans and mice. Neurobiology of Aging. 2002;23(4):565-78. doi: 10.1016/S0197-4580(02)00008-8.

45. Blankenship C, Zhang F, Keith R. Behavioral Measures of Temporal Processing and Speech Perception in Cochlear Implant Users. J Am Acad Audiol. 2016;27(9):701-13. Epub 2016/10/09. doi: 10.3766/jaaa.15026. PubMed PMID: 27718347; PMCID: PMC6921515.

46. Li B, Guo Y, Yang G, Feng Y, Yin S. Effects of Various Extents of High-Frequency Hearing Loss on Speech Recognition and Gap Detection at Low Frequencies in Patients with Sensorineural Hearing Loss. Neural Plast. 2017;2017:8941537. Epub 2018/02/16. doi: 10.1155/2017/8941537. PubMed PMID: 29445551; PMCID: PMC5763132.

47. Yuvaraj P, Jayaram M. Audiological Profile of Adult Persons with Auditory Neuropathy Spectrum Disorders. J Audiol Otol. 2016;20(3):158-67. Epub 2016/12/13. doi: 10.7874/jao.2016.20.3.158. PubMed PMID: 27942602; PMCID: PMC5144811.

48. Allen Brain Map. Neurotrophic tyrosine kinase, receptor, type 32020 June.

49. Knipper M, Van Dijk P, Nunes I, Ruttiger L, Zimmermann U. Advances in the neurobiology of hearing disorders: recent developments regarding the basis of tinnitus and hyperacusis. Prog Neurobiol. 2013;111:17-33. Epub 2013/09/10. doi: 10.1016/j.pneurobio.2013.08.002. PubMed PMID: 24012803.

50. Ison JR, Allen PD, O'Neill WE. Age-related hearing loss in C57BL/6J mice has both frequency-specific and non-frequency-specific components that produce a hyperacusis-like exaggeration of the acoustic startle reflex. J Assoc Res Otolaryngol. 2007;8(4):539-50. Epub 2007/10/24. doi: 10.1007/s10162-007-0098-3. PubMed PMID: 17952509; PMCID: PMC2538342.

51. Hayes SH, Radziwon KE, Stolzberg DJ, Salvi RJ. Behavioral models of tinnitus and hyperacusis in animals. Front Neurol. 2014;5:179. Epub 2014/10/04. doi: 10.3389/fneur.2014.00179. PubMed PMID: 25278931; PMCID: PMC4166233.

52. Sun W, Deng A, Jayaram A, Gibson B. Noise exposure enhances auditory cortex responses related to hyperacusis behavior. Brain Res. 2012;1485:108-16. Epub 2012/03/10. doi: 10.1016/j.brainres.2012.02.008. PubMed PMID: 22402030.

53. Sun W, Lu J, Stolzberg D, Gray L, Deng A, Lobarinas E, Salvi RJ. Salicylate increases the gain of the central auditory system. Neuroscience. 2009;159(1):325-34. Epub 2009/01/22. doi: 10.1016/j.neuroscience.2008.12.024. PubMed PMID: 19154777; PMCID: PMC2759817.

54. Fernandez KA, Jeffers PWC, Lall K, Liberman MC, Kujawa SG. Aging after noise exposure: acceleration of cochlear synaptopathy in "recovered" ears. J Neurosci. 2015;35(19):7509-20. doi: 10.1523/JNEUROSCI.5138-14.2015.

55. Stankovic KM, Corfas G. Real-time quantitative RT-PCR for low-abundance transcripts in the inner ear: analysis of neurotrophic factor expression. Hearing Research. 2003;185(1):97-108. doi: 10.1016/S0378-5955(03)00298-3.